Chapter 4
The Real Gas Closed Cycles

In practice, all the mechanical energy produced by thermal engines is generated via cycles that use steam (see Sect. 1.6) or combustion products (in gas-turbines and internal combustion engines). One consequence of using these fluids is that thermodynamic cycles operate in well-defined regions of the diagram of state (see Sect. 2.1): either along the limit curve (in the case of steam cycles) or far from the limit curve, in the region of ideal gas (in the case of single-phase gas cycles).

The chance to use fluids other than steam or air in closed cycles brings into play two different lines of development: (1) the use of fluids in the same physical state as steam and air, but with particularly favourable properties (for example, chemical inertness at high temperature, great molar mass or low vapour pressure at turbine inlet conditions), and (2) the use of fluids in a different state of aggregation from that in conventional states (liquid, steam, perfect gas), localising the thermodynamic cycles in nonconventional regions of the thermodynamic plane, for example, in Regions 3, 4, 6, 7 and 9 of Fig. 2.1 (see Sect. 2.1).

Examples of the first line of development include the Rankine cycles, with organic fluid vapours (see Chap. 3), which, although they too are realised along the limit curve, exploiting the benefits of the phase change, use organic fluids in place of water; alternatively, the cycles with liquid metals, discussed in Chap. 5; or, further, the closed gas-turbine cycle (see Sect. 1.7) and the Stirling engine (see Sect. 1.8), which use different single-phase fluids in the region of the ideal gas.

In Fig. 4.1, on the temperature–entropy plane, several possible cycle configurations are drawn. The cycle on the limit curve (cycle A) represents the conventional Rankine cycle with steam as working fluid. Cycle B, an ideal gas cycle, represents the traditional Brayton closed cycle, with inert gas. Cycle C, a real gas cycle, is a closed cycle that works at minimum temperatures and pressures close to the critical point,[1] in such a way as to bring into play important effects of real gas

[1] For these types of cycle, point 1 at the start of compression may be positioned indifferently to the right of the upper limit curve (as in the case shown in the figure) or to the left of the lower limit curve.

C.M. Invernizzi, *Closed Power Cycles*, Lecture Notes in Energy 11,
DOI 10.1007/978-1-4471-5140-1_4, © Springer-Verlag London 2013

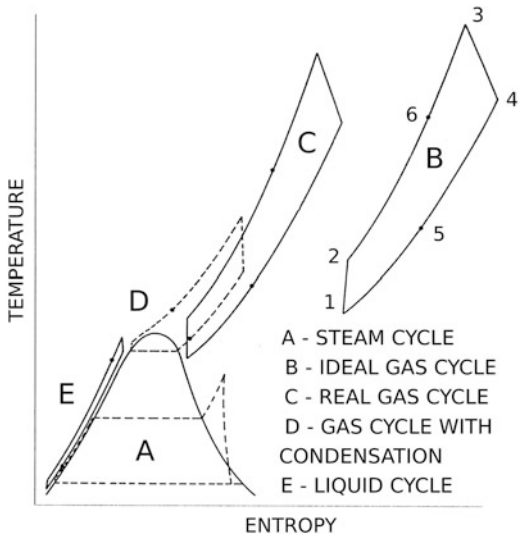

Fig. 4.1 Condensation thermodynamic cycles and single-phase thermodynamic cycles on the temperature–entropy plane. Each of the thermodynamic cycles represented uses different portions of the thermodynamic plane with different reduced temperatures and pressures

(discussed in Sects. 2.3 and 2.4). The gas and condensation cycle (cycle D) can be defined as a liquid phase compression gas cycle, in that the waste heat rejection takes place in the final zone of the saturation dome and the cycle extends almost completely into the region of the supercritical gas. Finally, the liquid cycle (cycle E) represents a thermodynamic cycle with a completely supercritical fluid in liquid phase as working fluid.

The thermodynamic cycles shown in Fig. 4.1 are characterised by isobaric and isentropic transformations, which represent the most common transformations for continuous flow machines (see Sects. 1.3 and 1.5). The Stirling cycles are not shown in the figure, but the same observations and conclusions apply to them, too (see Sect. 4.3).

The position of the cycle in the different regions of the thermodynamic plane, according to the various drawings in Fig. 4.1, once the thermodynamic conditions (temperature and pressure) of point 1 have been set, is a direct consequence of the values of temperature and critical pressure for the working fluid considered, that is, the values of reduced temperature $T_{r,1} = T_1/T_{cr}$ and reduced pressure $P_{r,1} = P_1/P_{cr}$ of point 1.

Figure 4.2a, for example, shows in the thermodynamic plane temperature–entropy, the saturation dome of three widely used fluids in industry, with similar molecular complexity: air ($T_{cr} = -140.7$ °C, $P_{cr} = 37.74$ bar), carbon dioxide ($T_{cr} = 31.06$ °C, $P_{cr} = 73.83$ bar) and water ($T_{cr} = 373.95$ °C, $P_{cr} = 220.64$ bar).

By virtue of the Law of Corresponding States (see Sect. 2.3), the three limit curves, rendered adimensional, converge into the single curve shown in Fig. 4.2b. Having set, by way of example, a temperature $T_1 = 25$ °C and a pressure $P_1 = 100$ bar, in the case of air, the corresponding point, in the reduced temperature–reduced entropy plane, falls within the region of the ideal gas (see Sect. 2.1); with a compressibility factor $Z \approx 0.97$, in the case of water, the point corresponds to the

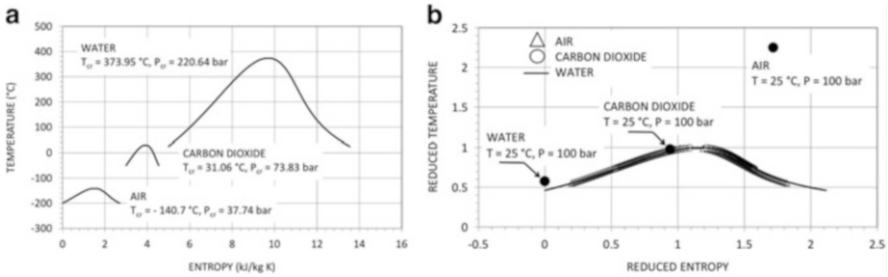

Fig. 4.2 (**a**) Limit curves for air, carbon dioxide and water in the temperature–entropy thermodynamic plane. (**b**) The same adimensional limit curves in accordance with the Law of Corresponding States

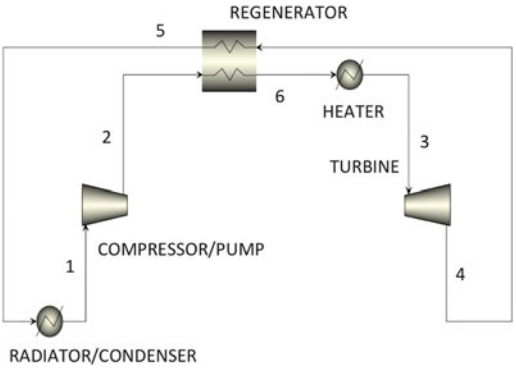

Fig. 4.3 Simplified scheme of the plant for a Brayton-type closed cycle. The scheme represents the thermodynamic cycles type C and E and the cycles type D of Fig. 4.1

thermodynamic conditions of a practically incompressible liquid and in the case of carbon dioxide the point falls very close to the critical point (see Fig. 4.2b) with a compressibility factor $Z \approx 0.25$, near the critical one. In the case of carbon dioxide, the thermodynamic conditions of the point at 25 °C and 100 bar are, therefore, characterised by the intense effects of the real gas, described in Sects. 2.2 and 2.4.

Therefore, each cycle shown in Fig. 4.1 can be realised, provided that the appropriate working fluid is chosen. In principle, then, specific thermodynamic cycles can be used for all the different applications that may be encountered.

The steam Rankine cycles are discussed in Sect. 1.6 and Chap. 3 is dedicated to the ORCs. The single-phase thermodynamic cycles with perfect gas are dealt with in Sect. 1.7 (the closed recuperated Brayton cycles) and in Sect. 1.8 (the Stirling cycles), whilst here we discuss the real gas closed Brayton cycles (cycle C of Fig. 4.1) and the liquid phase compression gas cycle (cycle D of Fig. 4.1). In fact, condensation has every right to be considered a real gas effect. Figure 4.3 represents the plant scheme to which we shall refer below.

A further effect of real gas, dissociation (Region 9 of Fig. 2.1), may also, in principle, be adequately exploited to create thermodynamic cycles [1, 2]. These

cycles will not be considered here: even though they are conceptually very interesting, the technology of dissociating gases has still to be completely tested. Dissociation at high temperatures (with a corresponding increase in the number of moli) and the recombination at low temperatures (with a corresponding reduction in the number of moli) make it possible to increase the work of expansion and reduce that of compression, thereby limiting one of the main causes of the modest performances in Brayton cycles with ideal gas. In fact, as discussed in Sect. 1.7 and as we shall see below, the efficiency losses correlated with the fluid dynamic losses on the turbomachinery are proportional to the sum of the compression and expansion power, which, in the case of the Brayton cycles with ideal gas, is far greater than the useful work. The reactions of dissociation and association of the molecules comprising the gas mixture also brings into play the latent heats of reaction, which benefit the heat exchange and increase the coefficients of heat transfer in the heat exchangers. The result of all this is good thermodynamic efficiency even at not particularly high temperatures (for example 500–600 °C compared to the 800 °C typical of the Brayton closed cycles with ideal gas) and, having set the power, smaller and more compact turbomachinery and heat exchangers than those commonly used in Brayton cycles with ideal gas and in Rankine cycles. On the other hand, the chemically reactive gases for use as working fluids in Brayton or Rankine cycles, N_2O_4 and NOCl, which manifest dissociation and recombination in temperature intervals between ambient and 800–1,000 °C, are toxic. Compatibility with materials, especially at high temperatures, is a second serious problem, since the fluids are reactive. A further problem is the rate of chemical reaction and the times needed for reaching equilibrium, which must be compatible with the times corresponding to the variations in pressure and temperature in the various engine components.

It is worth remembering that, in the years 1970–1980, the then Nuclear Power Institute of the Bielorussian SSR Academy of Sciences developed a mobile nuclear reactor, the "Pamir-630D", of 630 kW electric with nitrogen tetraoxide as the heat-carrying fluid. The reactor, cooled by air, could be transported on a truck.

In the following sections of this chapter, we shall examine (1) energy cycles with carbon dioxide, as an example of closed cycles with real gas as working fluids: cycle C of Fig. 4.1 and cycle D of Fig. 4.1; (2) organic real gas cycles; and (3) the Stirling engines, the performances of which, in principle, would also benefit significantly from the real gas effects.

4.1 Carbon Dioxide Power Cycles

Carbon dioxide was used as coolant in the Calder Hall nuclear power station in 1956 [3]. Later, completely supercritical power cycles (single phase, with minimum pressure greater than the critical pressure) were discussed by Feher in 1967 [4]. Angelino, in a series of papers, [5–8] dealt exhaustively with the thermodynamics of supercritical cycles with carbon dioxide, even suggesting plant modifications to improve their performance. More recently, [9–12], for nuclear reactors, the

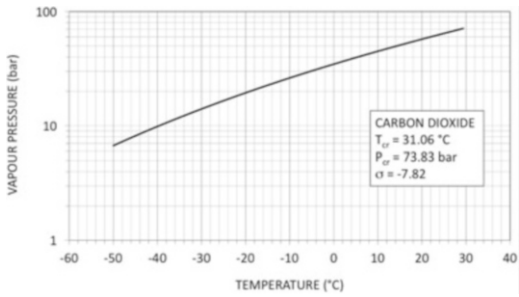

Fig. 4.4 Vapour pressure of the carbon dioxide as a function of temperature

supercritical carbon dioxide cycles have been re-proposed as an alternative to Brayton closed cycles with helium (see Sect. 1.7.7 and Exercise 1.8).

Carbon dioxide has a critical temperature of 31.06 °C, close to room temperature. As a result, the Brayton thermodynamic cycles with temperature T_1 of 20–30 °C and minimum pressures P_1 close to the critical pressure are characterised by compressibility factors that are a third/quarter of the corresponding compressibility factors for an ideal gas with the same minimum temperature and pressure. This considerably reduces the work spent in compression and gives a useful work that it still positive even though the maximum temperature of the cycle is not particularly high.

The vapour pressure of the carbon dioxide is given in Fig. 4.4: the pressure of the critical point is 73.83 bar. Therefore, the real gas Brayton cycles with carbon dioxide tend to have high minimum and maximum pressures. On the one hand, while the high density of the working fluid has beneficial effects on the size of the machinery (see Sect. 1.7.6), on the other, it could increase the costs of the materials employed. The internal efficiency of the turbomachinery tends to increase with the pressure, but, having set the power and the specific work, the number of revs also rises with the average operating pressure. As we shall see below, in the real gas Brayton cycles, too, regeneration is hard, which makes them inappropriate for conventional fossil power plants (due to the high stack heat losses they would incur).

The liquid phase compression gas cycle D in Fig. 4.1, having set the minimum temperature T_1, has a minimum pressure lower than that of a totally supercritical Brayton cycle (cycle B with pressure at the start of compression higher than the critical pressure), with very comparable efficiency, and represents a thermodynamic cycle with the advantage of the compression in the liquid phase (like Rankine cycles) and with the expansion in the gas region, thereby avoiding the need for superheating and re-superheating typical of the steam cycles (see Sect. 1.6). Compared to the Rankine cycle with steam, then, the liquid phase compression gas cycle has far lower expansion ratios and regeneration does not require the use of numerous exchangers typical of the steam cycles.

Figure 4.5 shows the results of cycle efficiency for ideal and real cycles (the performance of the ideal cycles are calculated with ideal components and in the absence of pressure losses), as the compression ratio r_C varies. The maximum temperature T_3 is always equal to 600 °C. The temperature T_1 has always been

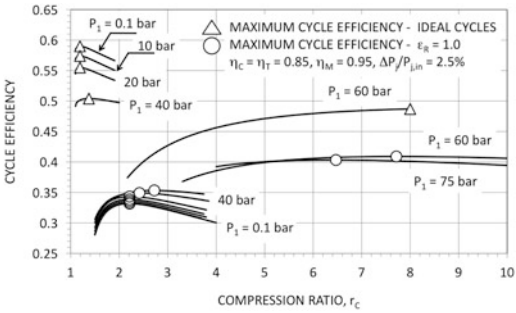

Fig. 4.5 Thermodynamic efficiency for Brayton closed cycles with carbon dioxide. In all cases, it was assumed $T_1 = 22\ ^\circ\text{C}$ and $T_3 = 600\ ^\circ\text{C}$

considered equal to that of condensation, at the pressure of 60 bar (about 22 °C, see Fig. 4.4). Thus, the cycle with P_1 equal to 60 bar represents a gas cycle with compression in the liquid phase, when P_1 is below 60 bar the Brayton cycles are to be considered in the zone of superheated gas and for pressures P_1 greater than the critical pressure, the Brayton cycles will be totally supercritical.

We chose a temperature T_1 that was lower than the critical temperature ($T_{r,1} = 0.97$) in order to analyse condensation cycles, too, and to emphasise the effects of the real gas in cycles with a single-phase fluid (Brayton cycles).

The same Fig. 4.5 also reports the cycle performance values for just the efficiency of the regenerator ϵ_R unit (for the definition of the regenerator efficiency, see Sect. 1.7.4, 1.35). In this case, the isentropic efficiencies η_C of compression and η_T of expansion are assumed to be 0.85 (the effect of reheating caused by fluid dynamic losses on the stages during expansion has been ignored for simplicity; see Sect. 1.7.3). Mechanical efficiency of the shaft has been considered as 0.95. The pressure loss on each exchanger has been considered equal to 2.5 % of the fluid pressure on entry into the component. There are two pressure losses on the regenerator: one on the low-pressure side and the other on the high-pressure side.

In the case of cycles containing just ideal components, it was observed that as the minimum pressure P_1 grows, the maximum efficiency of the cycle diminishes: the efficiency is 0.60 when $P_1 = 0.1$ bar for $r_C = 1.19$; it is 0.49 when $P_1 = 60$ bar for $r_C = 8$ (gas cycle with compression in the liquid phase).

The worsening of the thermodynamic quality of the ideal cycle as the pressure P_1 increases is the consequence of the negative effects of the real gas on the heat exchange in the regenerator. In fact, while the ratio between the net useful work and the total work $(W_T - W_C) / (W_T + W_C)$ increases significantly due to the positive effects of the real gas on the compressibility in the compression phase (see Fig. 4.6a), the notable difference in the specific heat at constant pressure between the high-pressure side and the lower-pressure side in the regenerator (see also Sect. 2.4, Fig. 2.4) introduces a temperature difference at the extremity greater than zero even when $\epsilon_r = 1$ (Fig. 4.6b).

Figure 4.6a shows the ratio between the net useful work $(W_T - W_C)$ and the total work $(W_T + W_C)$, under optimal performance conditions, passes from 0.46, in the case of an ideal gas, to 0.7 in the case of a liquid phase compression gas

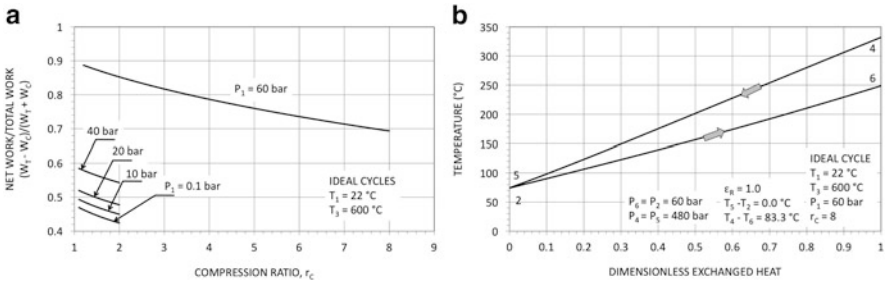

Fig. 4.6 Carbon dioxide ideal cycles, comparison between ideal gas and real gas (**a**) ratio between the useful work and the total work of turbomachinery (compressor and turbine); (**b**) diagram of heat exchange in the regenerator of an ideal cycle with compression in the liquid phase

cycle. Figure 4.6b reports the behaviour of the gas temperatures in the regenerator in the liquid phase compression gas cycle for the compression ratio $r_C = 8$. At the pressure of 60 bar, the average specific heat at constant pressure is 1,137 J/kg K, whilst, at the average pressure of 480 bar, the average specific heat is 1,677 J/kg K (48 % higher). The consequence is a temperature difference $(T_4 - T_6)$ which, rather than null, even with $\epsilon_R = 1$, stands at 83 °C. This introduces a thermodynamic loss which, in the case of ideal cycles where it is the only one present, penalises the cycle performance in the case of real gas compared to ideal gas.

The picture changes dramatically if we introduce the machine inefficiencies and the pressure losses. The results of cycle performance are shown in Fig. 4.5, for $\epsilon_R = 1$. The maximum cycle efficiency passes from 0.33 in the case of ideal gas, with a corresponding compression ratio of around 2.2, to 0.41 for the liquid phase compression gas cycle ($P_1 = 60$ bar con $r_C = 7.7$) and to 0.40 for the supercritical real gas Brayton cycle ($P_1 = 75$ bar with $r_C = 6.5$). In this case, the notable drop in thermodynamic losses on the work of the turbomachinery (the consequence of the increase in the ratio $(W_T - W_C) / (W_T + W_C)$, passing from the ideal gas to the real gas) improves the thermodynamic performances of the cycles with real gas, despite the adverse effect of the losses in regeneration.

Figure 4.7 illustrates the effects of the efficiency ϵ_R of the regenerator on the cycle performance for Brayton cycles with perfect gas and for cycles with compression in the liquid phase at $P_1 = 60$ bar.

The liquid phase compression gas cycles (although the conclusions are qualitatively valid also for the cycles C in Fig. 4.1 with real gas), suffer much less from the fall in efficiency ϵ_R than the cycles with ideal gas. For example, in the case of ideal gas cycles, when the efficiency of the regenerator ϵ_R passes from the unit value to 0.9, the maximum efficiency of the cycle drops by 25 %; in the case of the liquid compression gas cycles, the drop in the maximum efficiency is 10 % (in the intervals considered in the compression ratio r_C).

There is a comparison between the efficiency of the real gas supercritical Brayton cycles (cycle of type C in Fig. 4.1) and the liquid phase compression gas cycles (cycles of type D in Fig. 4.1) in Fig. 4.8. The figure also compares

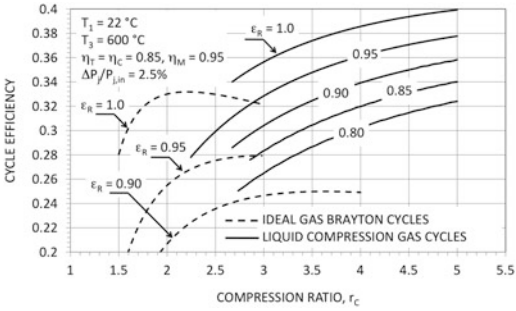

Fig. 4.7 Thermodynamic efficiency for Brayton closed cycles with carbon dioxide. Effect of the regenerator efficiency on the cycle performance

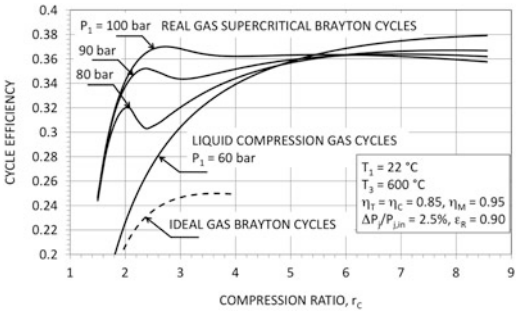

Fig. 4.8 Thermodynamic efficiency for Brayton closed cycles with carbon dioxide

the cycle performances with ideal gas. The maximum efficiency η for the liquid phase compression gas cycle is reached with very high compression ratios (in the case considered, the cycle efficiency eta reaches 38 % for $r_C = 8$); the totally supercritical Brayton cycles (with $P_1 = 80$, 90 and 100 bar) present a local maximum efficiency at low compression ratios (for instance, in the case with $P_1 = 90$ bar, $\eta = 0.35$ for $r_C = 2.3$) and a global maximum at high compression ratios (for instance, in the case with $P_1 = 90$ bar, $\eta = 0.36$ per $r_C = 6.0$).

This apparently anomalous thermodynamic behaviour is the direct consequence of the low temperature $T_{r,1}$ and is justifiable when we observe that, referring to the plant scheme in Fig. 4.3, the efficiency of the regenerator ϵ_R, in accordance with the definition given with (1.35), can be rewritten as

$$\begin{aligned}\epsilon_R &= \frac{H_6 - H_2}{H_4 - H_{5'}} \\ &= \frac{H_4 - H_5}{H_4 - H_{5'}} \\ &= \frac{H_4 - H_5}{(H_4 - H_5) + (H_5 - H_{5'})} \\ &\approx \frac{\overline{C}_{P,4-5}\,(T_4 - T_5)}{\overline{C}_{P,4-5}\,(T_4 - T_5) + \overline{C}_{P,5-5'}\,(T_5 - T_{5'})}\end{aligned} \tag{4.1}$$

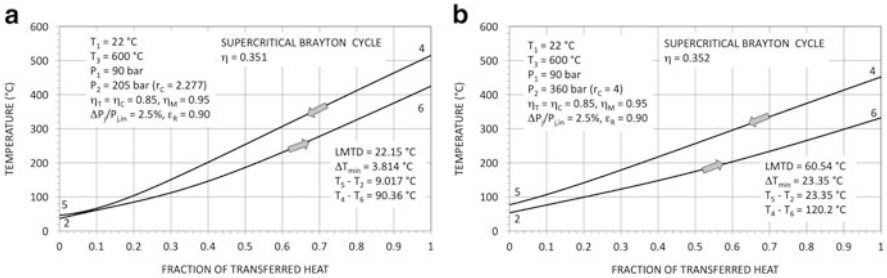

Fig. 4.9 Temperature trends in the regenerator of supercritical Brayton cycles with real gas. The pressure $P_1 = 90$ bar and the regenerator efficiency $\epsilon_R = 0.90$ are the same in both cases. (**a**) Cycle with modest compression ratio ($r_C = 2.28$). (**b**) Cycle with compression ratio $r_C = 4$. LMTD is the logarithmic mean temperature difference in the regenerator

with $\overline{C}_{P,4-5}$ the mean specific heat at constant pressure between point 4 and point 5 and $\overline{C}_{P,5-5'}$ the mean specific heat at constant pressure of the gas between point 5 and point 5′. Since $T_{5'} = T_2$, from (4.1) we get

$$T_5 - T_2 = (T_4 - T_5)\left(\frac{1}{\epsilon_R} - 1\right)\frac{\overline{C}_{P,4-5}}{\overline{C}_{P,5-5'}} \tag{4.2}$$

so, the temperature difference at the cold end of the regenerator, having set the efficiency ϵ_R, may also be a modest fraction of $(T_4 - T_5)$, according to the value of the ratio between the specific heats $\overline{C}_{P,4-5}/\overline{C}_{P,5-5'}$. The temperature difference $(T_5 - T_2)$ is then strictly correlated to the minimum temperature difference ΔT_{min} in the regenerator.

Just around the critical point, for $P_1 > P_{cr}$, when T_2, the temperature at the end of compression, is about 30–40 °C, the ratio $\overline{C}_{P,4-5}/\overline{C}_{P,5-5'}$ is significantly lower of the unit and $(T_5 - T_2)$ is small, with a ΔT_{min} that may turn out to be excessively low. See, for example, Fig. 4.9a.

Therefore, the heat exchange irreversibilities in the regenerator diminish rapidly with r_C due to the concomitant effect of a reduction in the Λ (logarithmic mean temperature difference) and a contemporary reduction in the power to regenerate per unit of useful work. As a consequence, the cycle efficiency grows rapidly as the compression ratio r_C increases.

However, with a rise in the compression ratio there also comes a rise in temperature T_2 and, from a certain point onwards, the ratio of the specific heats $\overline{C}_{P,4-5}/\overline{C}_{P,5-5'}$ starts rising again, to stabilise at more or less unitary levels. Consequently, the difference in temperature $(T_5 - T_2)$ grows, before diminishing slowly, stabilising at a more or less constant level. See, for example, Fig. 4.9b.

The thermodynamic irreversibility on the regenerator, anyway, continues to fall as r_C increases, but solely because the thermal power regenerated per unit of useful power is reduced. Figure 4.10, varying the compression ratio r_C, reports the thermodynamic losses (as a fraction of the maximum efficiency, see Exercise 1.2)

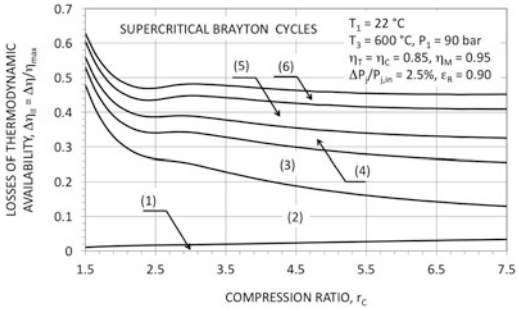

Fig. 4.10 Losses of thermodynamic availability as a function of the compression ratio r_C for supercritical Brayton cycles with carbon dioxide. (1) loss in compression, (2) loss on the regenerator, (3) loss associated with heat introduction, (4) loss in expansion, (5) loss on the radiator, (6) loss due to the mechanical efficiency of the power shaft

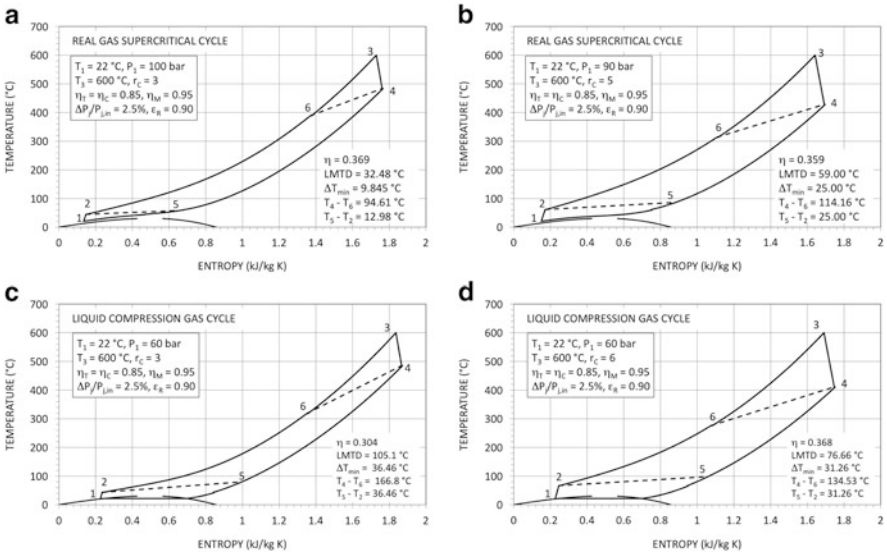

Fig. 4.11 Thermodynamic diagrams for several cycles with carbon dioxide in the temperature–entropy plane. (**a**) and (**b**) Supercritical Brayton cycles. (**c**) and (**d**) Cycles with compression in liquid phase

for a reference case. The figure clearly shows the diminution of the irreversibilities due to heat exchange in the regenerator: at first, very fast, then, after the inflexion (with r_C about 2.5), much more slowly.

Figure 4.11 reports two real gas supercritical Brayton cycles and two condensation cycles, on the T-S plane.

The supercritical Brayton cycles, in accordance with the results in Fig. 4.8, for relatively high pressures P_1, have good efficiency even at modest compression ratios

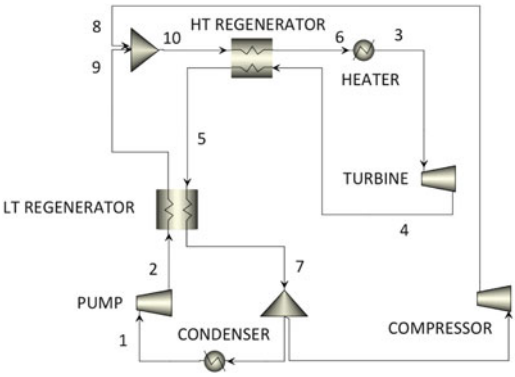

Fig. 4.12 Simplified plant scheme for cycle with partial condensation and split compression

(for example if $P_1 = 100$ bar, when $r_C = 3$ there is an efficiency η of around 0.37). In these conditions, though, the minimal temperature differences in the regenerator (due to effects linked to the rapid change in specific heats at constant pressure, discussed above) could be very small (about 10 °C, in the example in Fig. 4.11a). As the compression ratio increases, the temperature profiles in the regenerator become more regular; the efficiency is not too badly penalised by the high r_C, but the maximum pressures are very high (in the example of Fig. 4.11b, $P_1 = 90$ bar, $P_2 = 450$ bar, $\eta = 0.36$ with $\Delta T_{min} = 25$ °C).

The condensation cycles, with compression in the liquid phase and expansion starting from the supercritical gas zone, are characterised by good efficiency only at high compression ratios (in the example of Fig. 4.11d, the efficiency $\eta = 0.37$ for a compression ratio $r_C = 6$). In these cycles, the high specific heat at constant pressure of the compressed fluid compared to that of the gas exhausted by the turbine, always introduces a high thermodynamic irreversibility into the heat exchange at the level of the regenerator, in particular, at small compression ratios. In the example of Fig. 4.11c, for $r_C = 3$, we get $\Lambda = 105$ °C, with $(T_4 - T_6) = 167$ °C and $(T_5 - T_2) = 36$ °C, with an efficiency η of around 0.3. This difference in the specific heats between the regenerator fluids is responsible for the growing temperature difference between the hot fluid and the cold fluid in the heat exchanger, which, in the end, means heavily penalising the efficiency.

In the case of total condensation cycles, a substantial reduction in the irreversibilities in the regenerator is obtained by dividing the compression partly into a liquid phase and partly into a gas phase [7], according to the plant scheme in Fig. 4.12.

A balance in the thermal capacities can be achieved in the LT regenerator by dividing the low-pressure gas flow into two portions at point 7. If $\alpha = \dot{m}_1/\dot{m}_7$ represents the fraction of the flow that condenses, $1 - \alpha = \dot{m}_8/\dot{m}_7$ is the fraction directly compressed from the pressure P_7 of point 7 to the pressure P_8 of point 8. Having set the temperature differences at the ends $(T_7 - T_2)$ and $(T_5 - T_9)$, the α fraction of the flow can be calculated by the balance of power on the low temperature regenerator: $\alpha\,(H_9 - H_2) = (H_5 - H_7)$.

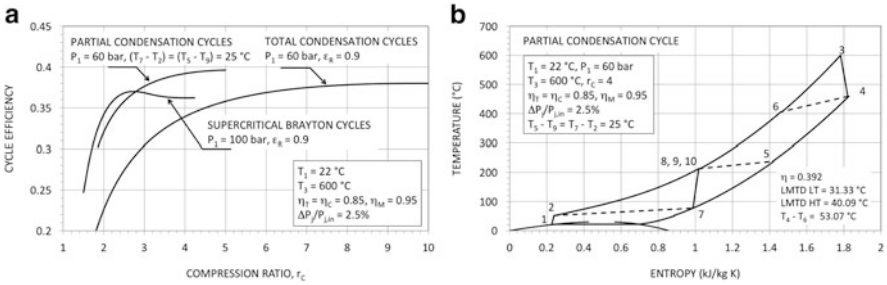

Fig. 4.13 (**a**) Cycle efficiency as a function of the compression ratio for supercritical Brayton cycles, cycles with total condensation and cycles with partial condensation. (**b**) Scheme of a partial condensation cycle in the temperature–entropy plane

The two flows, heated to temperatures $T_8 = T_9$ (one by the regenerator, the other by the compression), mix together and pass through the high temperature regenerator. The gas is heated in the heater from temperature T_6 to the maximum temperature T_3, expanding in the turbine up to point 4, then cooled first in the high temperature regenerator, then in the low temperature regenerator, down to temperature T_7: from where the cycle restarts.

Dividing the gas flow in point 7 has a similar effect to that of regeneration in the steam cycles. In the high temperature regenerator, the heat capacities of the two flows are not very different because of the elevated temperature, significantly higher than the critical temperature, which tends to lessen the effects of real gas (see Sect. 2.2).

Figure 4.13a compares the efficiency results of cycles with total condensation, with partial condensation and with completely supercritical Brayton cycles. The efficiency of cycles with partial condensation and split compression reach values close to 40 %. When $r_C = 4$, the efficiency of the cycle with partial condensation (shown on plane T-S in Fig. 4.13b) is about 0.39, compared with a value of 0.34 for the cycle with total condensation and compression entirely in the liquid phase.

Thermodynamic analysis has shown that to obtain the maximum thermodynamic benefits connected with the effects of real gas, it is necessary to make thermodynamic cycles with heat rejection and compression phase close to the critical point (see Fig. 4.8). In general, thermodynamic performance increases considerably if there is also present in the cycle a condensation phase (see Fig. 4.13), with expansion in the region of the supercritical gas.

Figure 4.14 represents the efficiency of the supercritical Brayton cycles as the minimum temperature T_1 varies. The temperature ratio T_3/T_1 is fixed at a value of 3 (ideal efficiency of 0.667). As we can see, even from a temperature T_1 of 40 °C (reduced temperature of 1.03), the positive effects of the real gas on the thermodynamics begin to diminish, in particular at low compression ratios.

For many aspects, carbon dioxide is effectively a good working fluid: its thermodynamic properties are well known, it is not toxic and it is abundant and

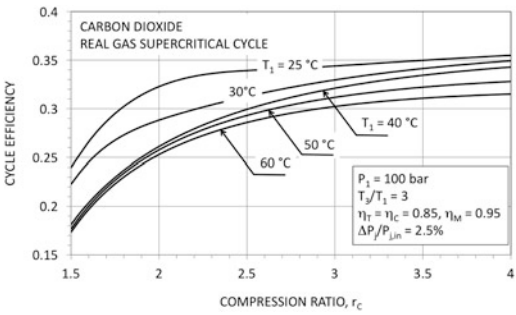

Fig. 4.14 Efficiency of supercritical Brayton cycles with carbon dioxide, as a function of the compression ratio and for different values of the temperature T_1 at the start of compression

inexpensive. The compatibility of carbon dioxide with materials should not be underestimated: it was thoroughly investigated during the development projects for the English nuclear reactors of Magnox and AGR [13], which were cooled with carbon dioxide. Serious problems of corrosion of the steel in the steam generators by carbon dioxide at 400 °C occurred in the Magnox-type reactor at Latina (Lazio, Italy).[2] On the other hand, the AGR reactors, made with stainless steel components, reached, in the few examples built, temperatures of 650 °C for the heat-carrying fluid (carbon dioxide), with operating pressures of 30–40 bar.

Studies into carbon dioxide corrosion are currently in progress, since the problem of carbon dioxide compatibility with construction and stainless steels at high, even supercritical, pressures is relevant today for the oil industry in oil pipelines and is fundamental for the technologies of carbon capture and storage. The presence of contaminants, like water, sulphur dioxide SO_2 and nitrogen dioxide NO_2, can exacerbate the phenomena of corrosion.

From a strictly thermodynamic point of view, one disadvantage is its critical temperature of 31.06 °C, which, in order to exploit properly all the benefits of the effects of a real gas, requires a low temperature cooling fluid, for example, water at 10–20 °C. With carbon dioxide thermodynamic cycles, even the evaporation towers could be inadequate if the climate is hot and humid.

Organic compounds offer a great variety of fluids, with highly varied critical temperatures, and careful selection may find working fluids with critical temperatures better suited than carbon dioxide. For example, critical temperatures around 30 °C for cycles producing just electricity, in places where water for cooling is widely available, and critical temperatures of 50–80 °C for CHP generation. The possibility of resorting to appropriate mixtures of organic fluids would also permit a continuous variation in the critical temperature, truly optimising the working fluid with respect to the sink temperature [14]. These aspects will be discussed in Sect. 4.2.

[2] A reactor with a nominal electrical power of 200 MW. Operative between 1963 and 1987. In 1969, the significant oxidisation of the mild steel in the steam generator by carbon dioxide forced them to reduce the maximum temperatures of the carbon dioxide to 360 °C, reducing the useful power by about 20 %.

4.2 Organic Real Gas Cycles

Table 4.1 lists several organic compounds with critical temperatures between 25 °C (HFC 23) and 150 °C (n-butane).

These can be used in Brayton cycles with notable real gas effects (and, in some cases, when convenient, cycles with compression in the liquid phase and expansion in the supercritical gas phase) that can meet various operating needs: either just the generation of electricity or combined electric and heat generation. The thermodynamic cycles that can be made are completely analogous to those described in Sect. 4.1 for carbon dioxide, except for the differences in the molecular complexity (the parameter σ described in Sect. 2.5) and the molar mass of the working fluid: as the molecular complexity rises, there is less cooling of the gas in the turbine during the expansion, having set the expansion ratio, with a consequent increase in the heat generated per unit of useful power; high molar masses correspond to moderate differences of enthalpy in compression and expansion, with the possibility of making single-stage turbomachinery that is very conservative from the point of view of mechanical stress on the blades.

Due to the high density of the fluid (a characteristic which is obviously true also for carbon dioxide and common to all those cycles with values of T_1 and P_1 close to the critical point), the dimensions of the turbomachines are limited, considering the high power levels (for example, average diameters of 0.2 m at 20–30 thousand revs for power of around one MW), or, alternatively, positive displacement engines can be made for lower power levels (10–100 kW).

However, the thermal stability limits the maximum operating temperatures of the organic fluids (see Sect. 3.2). Among the compounds listed in Table 4.1, the fluorocarbons HFC-23, HFC-125 and HFC-134a are, according to specific tests, unaffected by the temperature, at least up to 350–400 °C [14]. The hydrocarbons (ethane, propane and butane) are very unlikely to be stable at temperatures higher than 300–350 °C. With reference to HFC-125, Fig. 4.15 compares the efficiency of condensation cycles and totally supercritical cycles with carbon dioxide. In the examples discussed below, the minimum temperature T_1 is assumed to be 40 °C, considering the possibility of the surrounding air as cooling fluid. The advantage of being able to use a fluid that permits compression in the liquid phase is evident, both in terms of efficiency and the maximum pressures of the cycle.

Figure 4.16 compares two cycles with condensation at $T_1 = 40$ °C, operating with HFC-125. The cycle in Fig. 4.16a is a cycle with total condensation; that in Fig. 4.16b is with partial condensation. The maximum temperature T_3 is equal to 400 °C.

The partial condensation and the split compression significantly reduce the irreversibilities of the heat exchange in the regenerator (reducing the temperature differences between the hot fluid and the cold fluid, see Fig. 4.16c,d), with notable increases in the cycle efficiency.

Table 4.1 Critical temperature and pressure as well as molar mass for several organic compounds

Fluid	Critical temperature (°C)	Critical pressure (bar)	Molecular weight
Carbon dioxide	30.97	73.74	44.01
HFC 23[a]	25.82	48.36	70.014
Ethane	32.17	48.72	30.07
Sulphur hexafluoride	45.57	37.6	146.056
HFC 125[b]	66.02	36.15	120.022
R 218[c]	71.95	26.8	188.02
HFC 32[d]	78.11	58.05	52.024
Propane	96.68	48.72	44.097
HFC 134a[e]	101.11	40.59	102.032
Octafluorocyclobutane (C_4F_8)	115.22	27.78	200.031
Butane	151.97	37.96	58.123

[a]Trifluoromethane
[b]1,1,1,2,2-Pentafluoroethane
[c]Octafluoropropane (C_3F_8)
[d]Difluoromethane
[e]1,1,1,2-Tetrafluoroethane

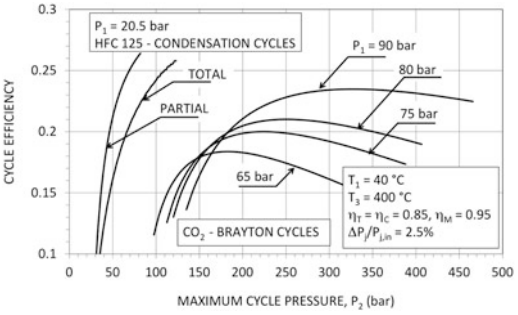

Fig. 4.15 Efficiency for cycles with HFC-125 and carbon dioxide as working fluids, as a function of the maximum pressure

Multi-Component Working Fluids

The possibility to mix working fluids with different critical temperatures will, in principle, enable the realisation of closed cycles with significant real gas effects for any minimum temperature T_1, not forgetting, though, the technological limit on the maximum temperature T_3 and bearing in mind all the considerations in Sect. 3.2.

Figure 4.17a represents several bubble and dew curves for mixtures of HFC-23 and HFC-125 and the envelope line of the points at maximum pressure as the fraction y_1 (molar fraction of HFC-23) varies: the critical temperature passes steadily from the value relative to pure HFC-23 (about 26 °C) to the value of

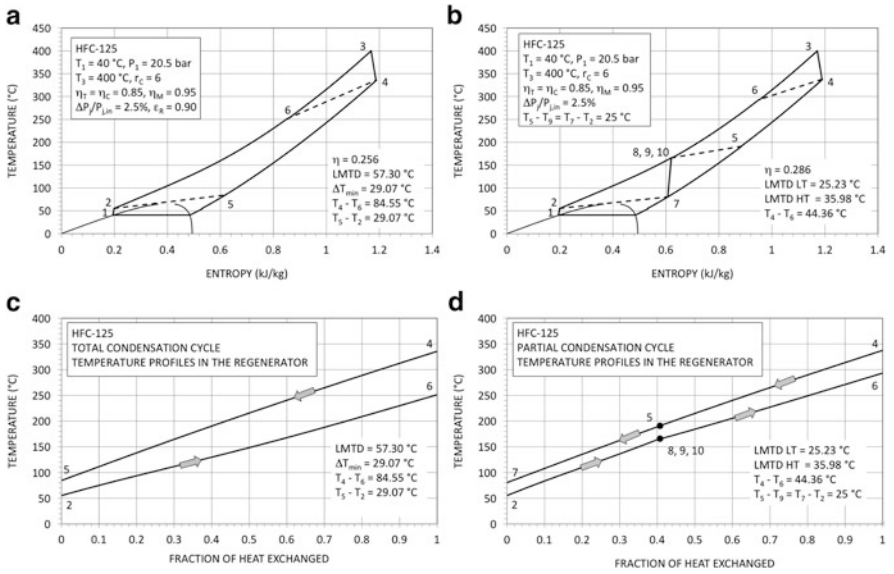

Fig. 4.16 Cycles with condensation and expansion in the supercritical gas phase, with HFC-125 as the working fluid on the temperature–entropy plane and diagrams of the heat exchange of the regenerator

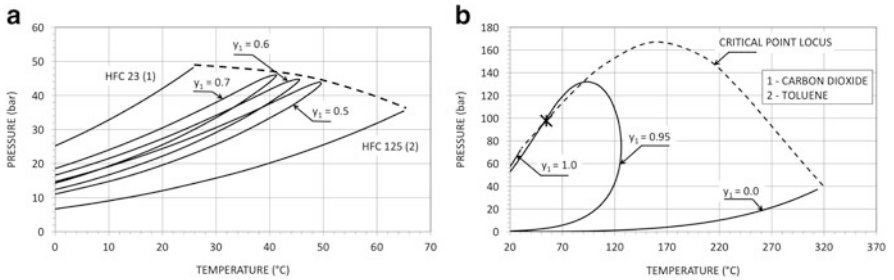

Fig. 4.17 Bubble and dew point curves for mixtures with different compositions. The equation used for the calculations is (2.5a) with the mixing rules (2.30). (**a**) Mixtures HFC-23 + HFC-125. The coefficient $\delta_{1,2} = -4.662409\,10^{-3}$ was obtained with a regression of the experimental data reported in [15]. (**b**) Mixtures carbon dioxide + toluene [16]

HFC-125 (66 °C). The figure traces the liquid–vapour equilibrium curves for three compositions: $y_1 = 0.7$, 0.6 and 0.5. Assuming $T_1 = 40$ °C, the mixture with $y_1 = 0.7$ enables supercritical Brayton cycles to be made with real gas effects; the mixtures with $y_1 = 0.6$ and 0.5 already enable the design of cycles with condensation. Condensation in non-azeotropic mixtures, though, is not isothermal: for instance, in the case of the mixture with $y_1 = 0.5$, the temperature glide (at the pressure of 37.5 bar) is 4.6 °C (the temperature during the condensation varies from 44.6 °C, in correspondence with the dew point, to 40.0 °C in correspondence with the bubble point).

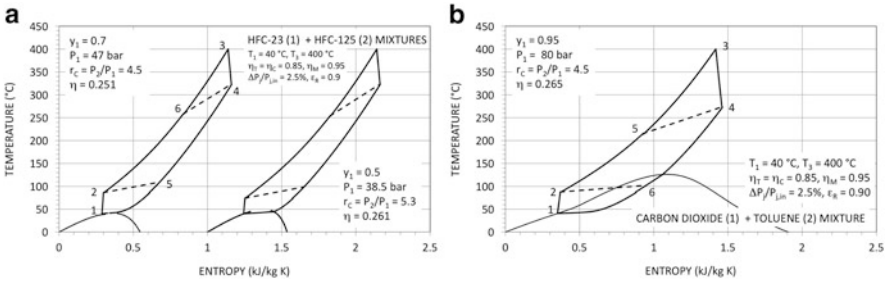

Fig. 4.18 Examples of supercritical Brayton cycles, with compression in the liquid phase for the mixtures. (**a**) Mixtures of HFC-23 + HFC-125. (**b**) A mixture of carbon dioxide + toluene [16]

Figure 4.17b reports the liquid–vapour equilibrium curves for mixtures of carbon dioxide and toluene (some physical properties of toluene are in Table 3.3). In this case, too, the critical point of the mixtures varies steadily (even though in an evidently non-linear fashion) between the values corresponding to the two pure fluids. Figure 4.17b shows the coexistence curve of the phases for the mixture with molar composition $y_1 = 0.95$ (carbon dioxide) and $y_2 = 0.05$ (toluene): the critical point of the mixture has a temperature around 55 °C and a pressure of about 98 bar; the point of maximum pressure (on the dew line, at about 132 bar) is at a temperature of 92 °C.

Figure 4.18a reproduces, on its thermodynamic plane T-S, two cycles with mixtures HFC-23 + HFC-125, while a gas cycle with compression in the liquid phase with carbon dioxide + toluene is shown in Fig. 4.18b.

Mixtures, therefore, constitute a valuable instrument for steadily varying the critical point of the working fluid, in such a way as to make Brayton cycles with real gas effects, for different applications with various minimum temperatures T_1. The variations in critical temperature and pressure with the composition of the mixture are not generally linear and experimental data and reliable calculation models are required to predict them. From a strictly thermodynamic point of view, there is a substantial similarity between totally supercritical Brayton cycles and condensation cycles, the choice depending on the applications (power levels, type of cooling fluid available etc.). The mixtures have heat exchange coefficients in condensation (and in evaporation) inferior to those of the corresponding pure fluids and this, in principle, favours (in the case of mixtures as working fluids) the use of totally supercritical Brayton cycles. The absence of two-phase flows, in certain particular cases, may prove beneficial in the design stage (for example, in space applications, in the absence of gravity). The choice of the mixture components has a direct influence on the design characteristics: for example, the cycle in Fig. 4.18b, has a minimum pressure of 80 bar and a maximum pressure of 360 bar and regeneration takes place partly with the two-phase flows and the glide temperature in condensation is high.

The Brayton cycles with real gas are characterised by large quantities of thermal power to be regenerated per unit of useful power, like in Brayton cycles with ideal gas (see Sect. 1.7). For example, for the cycle in Fig. 4.16a, $\dot{Q}_R / \left(\dot{W}_T - \dot{W}_C\right) = 5.6$

with a heat transfer parameter per unit of useful power $\dot{Q}_R/\Lambda\left(\dot{W}_T - \dot{W}_C\right) = 0.0972\ K^{-1}$. By comparison, a Rankine cycle with toluene (of the type shown in Fig. 3.9a) with $T_1 = 40\ °C$ and $T_4 = 400\ °C$, assuming the same component efficiencies and the same pressure losses, has, under the conditions of maximum efficiency, $\dot{Q}_R/\left(\dot{W}_T - \dot{W}_C\right) = 1.15$ and $\dot{Q}_R/\Lambda\left(\dot{W}_T - \dot{W}_C\right) = 0.0297\ K^{-1}$. The isentropic volume ratio of expansion of the Rankine cycle with toluene, though, is about 670 (140 times that of the cycle in Fig. 4.16a); another important difference is the isentropic work of expansion: 292 kJ/kg for the Rankine cycle, four times that of the cycle in Fig. 4.16a.

The gas cycles with real gas can be a valid alternative to closed Brayton cycles with an ideal gas. For example, the cycle in Fig. 1.42 (Brayton cycle with helium, at $T_1 = 20\ °C$ and $T_3 = 850\ °C$, with intercooling) has an efficiency of 40 %; the cycle with carbon dioxide in Fig. 4.13b has the same efficiency at a temperature $T_3 = 600\ °C$ (with relatively modest component efficiency and significant pressure losses).

The great thermal energy recovered in the regenerator per unit of useful power requires a demanding heat exchanger, at not particularly high maximum temperatures (400–700 °C), but with high operating pressures (in the order of 100 bar, in the range 100–300 bar). This requires the use of compact heat exchangers, made with pipes and plates of small diameter and width, to keep the matrix of heat exchange compact and light, but resistant to pressure differences even at high temperatures. A very promising technology appears to be that of PCHEs (printed circuit heat exchangers), which consist of channels of 2 mm diameter, chemically etched in metal sheets which are then diffusion bonded to create solid blocks, which are then welded together to make the complete heat exchanger [9, 17, 18].

Controlling the power in Brayton cycles with real gas may not be possible by simply varying the pressure levels in the system (as in Brayton cycles with ideal gas) and the control system should be designed appropriately, especially in the case of plant layouts that envisage split compression.

Exercises

4.1. Liquefied natural gas (LNG) is a natural gas cooled to −162 °C. At this temperature, the natural gas, at room pressure, condenses and becomes liquid. When it reaches a liquid state, natural gas occupies 600 times less space than in its gaseous state, making it possible to transport it over long distances and, under the form of LNG, it can easily be shipped at competitive prices from the producing countries to those in the world with the greatest demand. LNG is odourless, colourless, noncorrosive and non-toxic, with a density less than half that of water. It is expected that in years to come, the volumes of LNG being sold will be twice the current level.

Once it reaches its destination, the LNG is compressed, re-gasified and emitted into the network. An interesting option consists in using the cold LNG as a heat

sink for power cycles and exploiting its physical exergy to produce electricity. One example, with closed cycle and perfect gas, is discussed in Exercise 1.11. Here we shall discuss several thermodynamic condensation cycles with carbon dioxide and real gas Brayton cycles.

We imagine disposing of heat at a high temperature (generated by burning fuel), in such a way as to increase the conversion efficiency, increase the useful work per unit of re-gasified LNG and reduce the costs per unit of installed power. We suppose that the LNG is available as a supercritical gas at 70 bar (a typical value for long-distance gas pipelines).

The maximum useful power $\dot{W}_{\text{optimal}}$ obtainable from heating the LNG from the minimum temperature of −160 °C up to the ambient temperature of 25 °C can be derived from (B.4), assuming $\dot{S}_{\text{G}} = 0$ and with $\dot{E}_Q = 0$ and $T_0 = 298.15$ K this gives $\dot{W}_{\text{optimal}} = -443.196$ kW/kg/s. Having thermal power available at the temperature T_3 (higher than the temperature T_0 of the environment), (B.4) gives as a result:

$$\dot{W}_{\text{optimal}} = \frac{T_3}{T_0}\left[\left(\dot{E}_{\text{out}} - \dot{E}_{\text{in}}\right) - \left(1 - \frac{T_0}{T_3}\right)\dot{m}_{\text{LNG}}\left(H_{\text{out}} - H_{\text{in}}\right)\right]$$

which, for $T_3 = 600$ °C, gives $\dot{W}_{\text{optimal}} = -2825.56$ kW/kg/s.

Evaporation of the liquified gas may take place at the condenser of a supercritical cycle with carbon dioxide, but there needs to be a compromise between the high cycle efficiency (which would require the lowest possible condensation temperature) and the maximum use of the physical exergy of the LNG (which would require an elevated final temperature, only possible from a high condensation temperature, that is, a modest cycle efficiency). The Specific Power Performance Parameter (SPP, in MW/kg/s of LNG, see [19]), therefore, tends to grow with the condensation temperature, while the cycle efficiency increases regularly with the drop in the condensation temperature. Figure 4.19a has the results of efficiency and SPP for cycles with carbon dioxide. These are supercritical Rankine cycles with carbon dioxide (of the same type as those discussed previously, see Fig. 4.11c, but with condensation temperatures T_1 that are significantly lower than the critical temperature). The results relate to the hypothesis of using sea water in a sea water heater to preheat the carbon dioxide from temperature T_2, close to the condensation temperature (for example, −50 °C), up to a temperature (for example, 20 °C) close to room temperature. The efficiencies of the components and the parameters assumed for the calculations are those in Table 4.2.

At temperature $T_1 = -50$ °C, for example, corresponding to a maximum pressure $P_2 = 150$ bar, the cycle efficiency is around 0.52 and the SPP is 0.36. Figure 4.19b represents a thermodynamic cycle in the temperature–entropy plane. The simple cycle, adapted to the partial use of heat extracted from sea water, has good efficiency and the plant configurations are not too complex.

There is more detailed discussion of the performance of carbon dioxide condensation cycles, in the case of the particular application considered here, in [19], where we also talk about cycles with multiple condensation levels and compound cycles (of the type in Fig. 4.12), at high and low pressures.

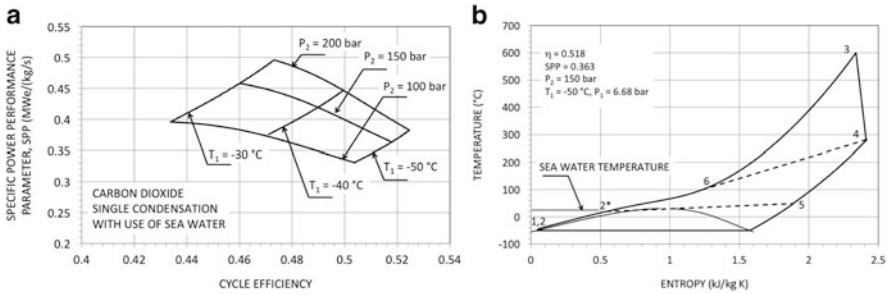

Fig. 4.19 Simple condensation cycles with carbon dioxide and with partial use of sea water. (**a**) Cycle efficiency and specific power output SPP. (**b**) Example of the cycle on the thermodynamic plane T-S

Table 4.2 Efficiencies of components and parameters assumed for the carbon dioxide cycles of Fig. 4.19

Turbine inlet temperature, T_3	600 °C
Condensation temperature, T_1	from −50 °C to −30 °C
Turbine adiabatic efficiency, η_T	0.90
Pump efficiency, η_C	0.70
Regenerator efficiency, ϵ_R	0.90
Logarithmic temperature difference in the condenser, Λ_C	50 °C
Mechanical efficiency, η_M	0.985
Alternator efficiency, η_A	0.98
Fractional pressure drops on each heat exchanger, $\Delta P_j / P_{j,in}$	2.5 %

In any case, the supercritical LNG, re-gasifying at variable temperatures, would be difficult to match with the condensation of a Rankine cycle, unlike the Brayton cycles, in which the heat is discharged as the temperature drops.

4.2. The ideal gas closed cycle has the potential to use almost completely the cooling capacity of supercritical LNG available at −160 °C and at supercritical pressures (for example, 70 bar; see Exercise 4.1). An alternative to using the closed Brayton cycle with perfect gas is the closed real gas Brayton cycle which, as we have seen in this section, is characterised by a drastically reduced work of compression that, to some degree, makes these cycles similar to the Rankine cycles. The significant reduction in the compression work guarantees good cycle efficiency even at less than high maximum temperatures. Important effects of the real gas on the compression become manifest, though, only in proximity of the critical point (for example, when $T_{1,r} = 0.98 - 1.01$), and this is the reason why, in usual applications, the permanent gases (air, nitrogen, helium) do not show any appreciable effects of the real gas at ordinary temperatures (see Fig. 4.2b). The situation is different if the closed gas cycle operates with minimum cryogenic temperatures, as in the case of the re-gasification process of LNG. Table 4.3 lists some of the substances that, in principle, could be used to make real gas Brayton cycles at temperatures T_1 close to that of the LNG.

Table 4.3 Critical temperature and pressure as well as molar mass for several working fluids in cryogenic Brayton cycles

Fluid	Critical temperature (K)	Critical pressure (bar)	Molecular weight
Nitrogen	126.2	33.98	28.014
Air	132.52	37.66	28.96
Argon	150.86	48.98	39.948
Oxygen	154.58	50.43	31.999
Methane	190.56	45.99	16.043

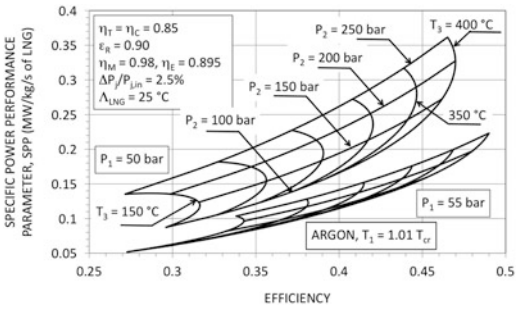

Fig. 4.20 Specific Power Performance Parameter (SPP, useful power per unit mass flow of vaporised LNG) for argon cycles and cycle efficiency for different minimum pressures and maximum pressures and temperatures

The modest compression work due to the relative incompressibility of the real gas is accompanied, though, by a fall in the end of compression temperature T_2 and, consequently, by a modest temperature T_5 (see Fig. 4.11a,b). This has the negative effect (in the case of the particular application considered here) of reducing the SPP specific power parameter.

Figure 4.20 reports the SPP Parameter (SPP) and the efficiency of real gas Brayton cycles with argon ($T_1 = 1.01 T_{cr}$) under different operating conditions. Passing from a minimum pressure P_1 of 50 bar to a P_1 of 55 bar, the cycle efficiency increases by an average of 2–3 points, but the SPP parameter drops significantly. For example, in correspondence with $T_3 = 350$ °C and $P_2 = 200$ bar, when $P_1 = 50$ bar the efficiency is 0.446 and the SPP is 0.289 MW/kg/s; when $P_1 = 55$ bar, we have a cycle efficiency of 0.46 and an SPP of 0.177 MW/kg/s (60 % lower): it is usually necessary to make a compromise between high efficiency values and acceptable values of the SPP parameter.

It is worth noting how, at even relatively modest T_3 temperatures (150–200 °C), the cycle efficiency is interesting. For example, it is the same at 0.316 with $P_1 = 50$ bar and $T_3 = 150$ °C, but with SPP = 0.123 MW/kg/s. This would permit the use of easily recovered low-grade heat as heat source, allowing a real gas Brayton cycle to be used (with small expansion ratios, for example, equal to 3), in place of an ORC. There is more detailed discussion of the potential of real gas Brayton cycles associated with the re-gasification of LNG in [20].

In this case, too, we should not overlook the possibility of mixing different gases (for example, argon and nitrogen) in such a way as to obtain a variation in the critical point and, thereby, broaden the choice of operating conditions.

4.3. Still with reference to the integration of real gas Brayton cycles into the re-gasification process of LNG, we consider the case of a "binary" cycle obtained with a commercial gas turbine of 4,600 kW (Mercury 50, a recuperated gas-turbine generator set) and with an argon "bottoming" cycle.

The characteristics of the gas turbine are the following: exhaust mass flow 63,700 kg/h, heat rate 9,351 kJ/kWh and exhaust temperature 377 °C. We consider a recovery cycle with argon with $T_1 = 1.01T_{cr}$, $T_3 = 350$ °C, $P_1 = 50$ bar and a compression ratio r_C of 4.5. The characteristics of the components are those reported in Fig. 4.20.

Assuming we can cool the exhaust gases of the gas turbine down to 100 °C, we get a power of the real gas Brayton cycle of 2,360 kW, an overall efficiency of 0.58 and an SPP of 0.90.

4.3 Real Gas Stirling Engines

The thermodynamics of ideal gas Stirling engines have been discussed in Sect. 1.8. In modern Stirling engines, the working fluid is typically helium or hydrogen, because of their good heat exchange properties, see Sect. 1.7, but there are severe sealing problems. Air has been proposed repeatedly for engines with a simple design, low rev and with modest specific power [21]. In any case, the working fluid employed operates in thermodynamic conditions that oblige it to behave as an ideal gas.

In the case of Stirling engines, as in Joule–Brayton engines, the use of real gas brings about a noticeable increase in the specific work and guarantees a discrete efficiency even at maximum operating temperatures that are inferior to those typical of perfect gas engines.

The Malone[3] engine was the first engine, regenerative and with external combustion, similar to the hot-air Stirling engine, which employed water as its working fluid in place of air. In the Malone engine, the very low compressibility of the fluid led to very high maximum pressures (800–1,000 bar), with very low rotational speed

[3]John Fox Jennens Malone, an Englishman, was born at Wallsend on Tyne in 1880 and died in 1959 at Newcastle upon Tyne. At eighteen years of age he entered the merchant navy and served for fourteen years. In the 1920s, he began to test heat engines with liquids as the working fluids and, in 1927, he completed a small water engine of 50 HP. Malone wrote in 1931 that "Trials by three different independent engineers gave 27 % indicated efficiency" [22] (a value that was two to three times greater than that of the steam engines used at the time on ships and locomotives). In 1932, Malone founded the Malone Instrument Co. Ltd, but his engine with liquid as its working fluid enjoyed no success, thanks also to the rapid growth of the high powered steam turbines and the internal combustion engines. In a letter of 1939, Malone gave vent to his bitterness: "there is one fact, a study of liquids as mediums in thermodynamics will teach an engineer more about the art of thermodynamics than all the universities on earth, or the memory men who infest them, and knowledge for knowledge's sake is better than their parasitical life" [23].

(30–300 rpm) and with small swept volumes of the pistons. Malone tried out various working fluids, among which is carbon dioxide [24].

The approach taken by Malone (followed later by other authors [25, 26]), in principle, makes it possible to create heat engines with liquid as a working fluid, positioning the expansion in proximity of the critical point, in Region 6 of Fig. 2.1, and the compression in Region 5 of Fig. 2.1 as, for example, the thermodynamic liquid cycle E in Fig. 4.1.

In fact, the useful power of a Stirling engine may be calculated as $\dot{W} = -P\left(\mathrm{d}V_\mathrm{C}/\mathrm{d}t + \mathrm{d}V_\mathrm{E}/\mathrm{d}t\right) = -P\,\mathrm{d}V/\mathrm{d}t$, with V representing the total instantaneous volume of the engine. The pressure $P = P(t)$ over time is not easy to calculate (see Sect. 1.8.1). Qualitatively, assimilating the engine to a closed system, at an appropriate average temperature, the pressure can be easily derived from the single equation (A.1) of the balance of mass: $\mathrm{d}M_\mathrm{tot}/\mathrm{d}t = 0$, with $M = \rho V(t)$. Or:

$$\frac{\mathrm{d}\rho}{\mathrm{d}t}V + \rho\frac{\mathrm{d}V}{\mathrm{d}t} = 0 \quad \text{with}$$

$$\frac{\mathrm{d}\rho}{\mathrm{d}t} = \left(\frac{\partial\rho}{\partial P}\right)_T \frac{\mathrm{d}P}{\mathrm{d}t} + \left(\frac{\partial\rho}{\partial T}\right)_\mathrm{P} \frac{\mathrm{d}T}{\mathrm{d}t} \quad \text{in which}$$

$$\frac{\mathrm{d}T}{\mathrm{d}t} = \left(\frac{\partial T}{\partial P}\right)_S \frac{\mathrm{d}P}{\mathrm{d}t}$$

$$= (-1)\,\frac{T}{\rho^2 C_\mathrm{P}}\left(\frac{\partial\rho}{\partial P}\right)_T \frac{\mathrm{d}P}{\mathrm{d}t} \quad \text{for an adiabatic expansion or compression or}$$

$$\frac{\mathrm{d}T}{\mathrm{d}t} = 0 \quad \text{for a isothermal expansion or compression}$$

So, for instance, with reference to an isothermal transformation, we get

$$\left(\frac{\partial\rho}{\partial P}\right)_T \frac{\mathrm{d}P}{\mathrm{d}t}V + \rho\frac{\mathrm{d}V}{\mathrm{d}t} = 0 \quad \text{or}$$

$$\frac{\mathrm{d}P}{\mathrm{d}t} = (-1)\,\rho\frac{\mathrm{d}V}{\mathrm{d}t}\,\frac{1}{V\left(\frac{\partial\rho}{\partial P}\right)_T}$$

The tendency of the engine pressure is, therefore, strictly correlated to the compressibility $(\partial\rho_\mathrm{P}) = (\partial\rho/\partial P)_T$. For a liquid under normal conditions (with $T = T_K$ close to room temperature) $(\partial\rho_\mathrm{P})$ is very small (null, if the liquid was rigorously incompressible); on the contrary, for a liquid with $T = T_\mathrm{H}$ close to the critical temperature, $(\partial\rho_\mathrm{P})$ is significantly greater than zero. The result is that even a working fluid in the liquid phase can guarantee finite variations of volume (modest, but not infinitesimal) with similarly finite pressures (although tending to be very high), with a net useful work on the cycle.

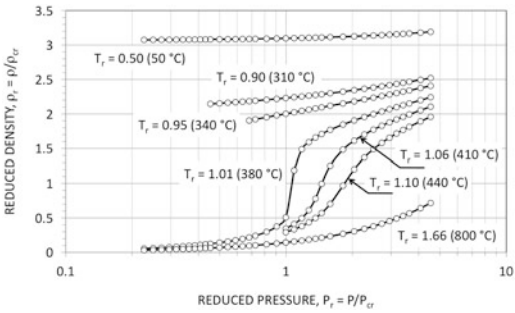

Fig. 4.21 Reduced density ρ_r as a function of the reduced pressure P_r in correspondence with different reduced temperatures T_r. The data refer to water [27]

Figure 4.21 reports reduced density values ρ_r, at different reduced pressures and reduced temperatures. Although the data in the figure refers to water, the trend of the reduced density as T_r and P_r vary, is, by the Law of Corresponding States (see Sect. 3.2), of general validity. Figure 4.21 clearly shows the great variations in the density as pressure varies in proximity to the critical temperature.

In the case of an engine with liquid as its working fluid, the variations of volume V, necessarily modest, imply small values of the expansion swept volume $V_{SW,E}$, small values of the ratio $\kappa = V_{SW,C}/V_{SW,E}$ and relatively large ratios $\zeta = V_D/V_{SW,E}$. Of greater interest for the application point of view, is an engine that uses a gas, but with significant real gas effects. In such a case, reducing the average compressibility of the fluid enclosed within the volume $V = V(t)$ of the engine, compared to the case with ideal gas, for similar volume variations, increases the average pressure anyway, with a significant increase in the work parameter $W^* = W/P_{max}V_T$.

The thermodynamic model described in Sect. 1.8.1 will now be applied to Stirling cycles with real gas and ideal gas. The design parameters are the usual ones: the phase angle ϕ, the ratio between the maximum temperature and the minimum temperature $\tau = T_H/T_K$, the ratio between the swept compression volume and the swept expansion volume $\kappa = V_{SW,C}/V_{SW,E}$, the ratio between the dead volume and the swept expansion volume $\zeta = V_D/V_{SW,E}$, the number of revs N, the efficiency of compression η_C and of expansion η_E (defined according to (1.62) and (1.63)), the fractional temperature difference in the regenerator ϵ defined by the condition (1.60) and by (1.61). For the calculations carried out below, the values reported in Fig. 4.22a have been assumed for the design parameters.

The results (valid within the limits of the calculation model used) for the comparison of engine performance are the work parameter $W^* = W/P_{max}V_T$ and the (indicated) efficiency of the engine $\eta = W/\oint \dot{Q}_H dt = W/Q_H$ (see Sect. 1.8.1).

The geometric parameters of the engine listed earlier also define the ratio between the dead volume V_D and the total volume V_T:

$$\frac{V_D}{V_{SW,E}} = \zeta \quad \text{and}$$

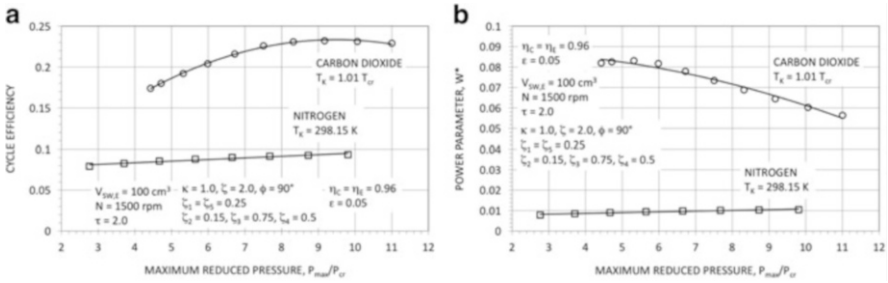

Fig. 4.22 Comparison between the thermodynamic performance of Stirling engines with nitrogen and with carbon dioxide. (**a**) Cycle efficiency as a function of the maximum reduced pressure of the cycle. (**b**) Work parameter W^*

$$\frac{V_\mathrm{T}}{V_{SW,E}} = 1 + \kappa + \zeta \quad \text{so,}$$

$$\frac{V_\mathrm{D}}{V_\mathrm{T}} = \frac{\zeta}{1 + \kappa + \zeta}$$

Then:

$$\begin{aligned}\frac{V_\mathrm{D}}{V_{SW,E}} &= \zeta \\ &= \frac{V_{CL,C}}{V_{SW,E}} + \frac{V_K}{V_{SW,E}} + \frac{V_\mathrm{R}}{V_{SW,E}} + \frac{V_\mathrm{H}}{V_{SW,E}} + \frac{V_{CL,E}}{V_{SW,E}} \\ &= \sum_{i=1}^{5} \zeta_i\end{aligned}$$

and, having set the four values of ζ_i, from the previous equation, we can derive the fifth. In the calculations that follow below, the fractions ζ_i that were assumed are listed in Fig. 4.22a.

The cycle efficiency with carbon dioxide (see Fig. 4.22a) reaches a maximum value of around 23 % in correspondence with a maximum pressure of about 9 times the critical pressure. The maximum efficiency, in the range of maximum reduced pressures considered, is 2.3 times greater than the value of the efficiency of cycles with nitrogen (ideal gas). The maximum values of the work parameter W^* for carbon dioxide (see Fig. 4.22b) are reached with maximum pressures between 4.5 and 6 times the critical pressure and are higher than the corresponding values for nitrogen by about 8.3 times.

Compared to the nitrogen cycles, the carbon dioxide cycles have optimal efficiency, although the temperature T_H, having assumed a ratio $\tau = T_\mathrm{H}/T_K = 2$, is

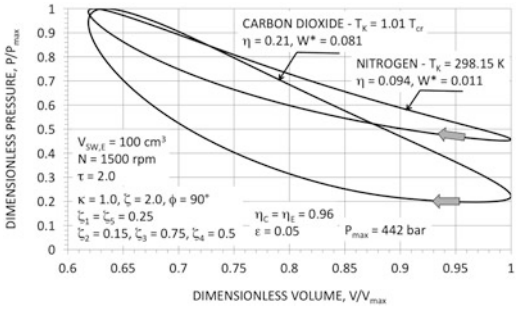

Fig. 4.23 Pressure–volume diagrams for carbon dioxide cycles and nitrogen cycle. For the carbon dioxide cycle, $T_K = 1.01 T_{cr}$ and for the nitrogen cycle, $T_K = 298.15$ K. The maximum pressure in both cases is 442 bar

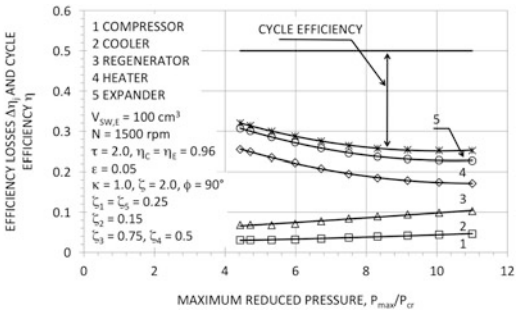

Fig. 4.24 Efficiency losses and cycle efficiency as maximum reduced pressure varies. The working fluid is carbon dioxide. The temperatures T_K and T_H and the parameters used for the calculations are the same as those used for Fig. 4.22a

relatively modest (341 °C for cycles with carbon dioxide and 323 °C for cycles with nitrogen). This is a consequence of the effects of real gas which, having localised the temperature T_K and the minimum pressure in proximity to the critical point of carbon dioxide, are responsible for a large pressure variation $(P_{max} - P_{min})/P_{mean}$: 1.51 in the case of the carbon dioxide cycle of Fig. 4.23 and 0.81 in the case of the nitrogen cycle.

The existence of the maximum efficiency value of Fig. 4.22a for the carbon dioxide cycles is explained by entropic analysis, which enables us to calculate the efficiency losses $\Delta\eta_j = T_0 \dot{S}_{G,j}/\dot{Q}_{in}$ reported in Fig. 4.24 (for the calculation, see Exercise 1.3, Appendix A.4 and C.3). The maximum efficiency value is a consequence, firstly, of the substantial and rapid diminishing of thermodynamic losses in the regenerator as the maximum pressure increases and then, by ever-increasing maximum pressures, of the prevalence of compressor and cooler losses.

So, the considerations are similar for the real gas Stirling engines to those of the real gas Brayton cycles: (1) they have good efficiency at high specific useful power; (2) there is the possibility of using multicomponent working fluids in order to control the critical temperature and meet, in principle, various operating needs; (3) good efficiency is obtained even with not particularly high maximum temperatures (with significant technological advantages in the choice of materials); and on the downside, (4) the maximum pressures which interest us are significantly higher than the critical pressure and, therefore, tend to be rather high (several hundred bars). On the other hand, the high pressures, the temperature close to the

critical temperature and the compressibility factors Z well below the unit, can prove beneficial and the ratio $\dot{W}_f / \dot{Q}$, between the power spent in overcoming the pressure losses and the thermal power exchanged in a heat exchanger (see (1.40) and the relative discussion), can also turn out to be ten times lower than the typical value for an ideal gas.

References

1. Krasin AK, Nesterenko VB (1971) Dissociating gases: a new class of coolants and working substances for large power plants. Atom Energ Rev 9(1):177–194
2. Angelino G (1979) Performance of N_2O_4 gas cycles for solar power applications. Proc Inst Mech Eng 193(1):313–320
3. Anonymous (1956) Calder Hall power Station. The Engineer, 5 October, pp 464–468
4. Feher EG (1967) The supercritical thermodynamic power cycle. In: Advances in energy conversion engineering. Intersociety energy conversion engineering conference, Miami Beach, FL, pp 37–44, 13–17 August
5. Angelino G (1967) Perspectives for the liquid phase compression gas turbine. J Eng Power Trans ASME 89(2):229–237
6. Angelino G (1967) Liquid-phase compression gas turbine for space power applications. J Spacecraft Rockets 4(2):188–194
7. Angelino G (1968) Carbon dioxide condensation cycles for power production. J Eng Power Trans ASME 90(3):287–295
8. Angelino G (1971) Real gas effects in carbon dioxide cycles. Atomkernenergie (ATKE) 17(1):27–33
9. Dostal V, Driscoll MJ, Hejzlar P, Wang Y (2004) Supercritical CO_2 cycles for fast gas-cooled reactors. In: Proceedings of ASMETurbo Expo 2004. Power for land, sea, and air, Vienna, Austria, 14–17 June. Paper GT2004–54242
10. Hejzlar P, Pope MJ, Williams WC, Driscoll MJ (2005) Gas cooled fast reactor for generation IV service. Progr Nucl Energ 47(1–4):271–282
11. Dostal V, Hejzlar P, Driscoll MJ (2006) High-performance supercritical carbon dioxide cycle for next-generation nuclear reactors. Nucl Tech 154:265–282
12. Dostal V, Hejzlar P, Driscoll MJ (2006) The supercritical carbon dioxide power cycle: comparison to other advanced power cycles. Nucl Tech 154:283–301
13. Lee JC, Campbell J Jr, Wright DE (1981) Closed-cycle gas turbine working fluids. J Eng Power Trans ASME 103:220–228
14. Angelino G, Invernizzi C (2001) Real gas Brayton cycles for organic working fluids. Proc IME J Power Energ 215(1):27–38
15. Lim JS, Park JY, Lee BG (2000) Vapor-Liquid Equilibria of CFC alternative refrigerant mixtures: trifluoromethane (HFC-23) + difluoromethane (HFC-32), trifluoromethane (HFC-23) + pentafluoroethane (HFC-125), and pentafluoroethane (HFC-125) + 1,1-difluoroethane (HFC-152a). Int J Thermophys 21(6):1339–1349
16. Invernizzi C M, van der Stelt T (2012) Supercritical and real gas Brayton cycles operating with mixtures of carbon dioxide and hydrocarbons. Proc IME J Power Energ 226(5):682–693
17. Nikitin K, Kato Y, Ngo L (2006) Printed circuit heat exchanger thermal-hydraulic performance in supercritical CO_2 experimental loop. Int J Refrig 29:807–814
18. Min JK, Jeong JH, Ha MY, Kim KS (2009) High temperature heat exchanger studies for applications to gas turbines. Heat Mass Trans 46:175–186
19. Angelino G, Invernizzi CM (2009) Carbon dioxide power cycles using liquid natural gas as heat sink. Appl Therm Eng 29:2935–2941

20. Angelino G, Invernizzi CM (2011) The role of real gas Brayton cycles for the use of liquid natural gas physical exergy. Appl Therm Eng 31:827–833
21. Organ A J (2007) The air engine. Stirling cycle power for a sustainable future. Woodhead Publishing Limited, Cambridge
22. Anonymous (1993) John Malone and the invention of liquid-based engines. Los Alamos Sci 21:117
23. Sier R (2007) John Fox Jennens Malone. The liquid Stirling engine. L A Mair, Chelmsford
24. Malone JFJ (1931) A new prime mover. J Roy Soc Arts 79(4099):679–709
25. Allen PC, Knight WR, Paulson DN, Wheatley JC (1980) Principles of liquids working in heat engines. Proc Natl Acad Sci Unit States Am 77(1):39–43
26. Swift GW (1989) A Stirling engine with a liquid working substance. J Appl Phys 65(11): 4157–4172
27. Parry WT, Bellows JC, Gallagher JS, Harvey AH (2000) ASME international steam tables for industrial use. CRTD-Vol. 58. ASME Press, New York, NY